Neural network identification of water pipe blockage from smart embedded passive acoustic measurements

Baronti, Luca; Castellani, Marco; Hefft, Daniel; Alberini, Federico

DOI:
10.1002/cjce.24202

Received: 17 October 2020 | Revised: 25 March 2021 | Accepted: 25 March 2021

DOI: 10.1002/cjce.24202

THE CANADIAN JOURNAL OF CHEMICAL ENGINEERING

Canadian Society for Chemical Engineering | For Our Future
Société canadienne de génie chimique | Pour notre avenir

ARTICLE

Neural network identification of water pipe blockage from smart embedded passive acoustic measurements

Luca Baronti[1] | **Marco Castellani**[2] | **Daniel Hefft**[3] | **Federico Alberini**[3]

[1]School of Computer Science, University of Birmingham, Birmingham, UK

[2]Department of Mechanical Engineering, University of Birmingham, Birmingham, UK

[3]School of Chemical Engineering, University of Birmingham, Birmingham, UK

Correspondence
Federico Alberini, School of Chemical Engineering, University of Birmingham, Birmingham, UK.
Email: f.alberini@bham.ac.uk

Abstract

This study presents a new neural network approach to identify the presence and type of obstruction in pipes from measurements of passive acoustic emissions. Inserts were used in a fluid re-circulation loop to simulate different types of blockage at various flow rates within the turbulent regime, generating patterns of acoustic emissions. The data were pre-processed using Fourier analysis, and two candidate sets of statistical descriptors were extracted for each measurement. The first set used average and spread of the Fourier transform amplitudes, the second used data binning to obtain a concise representation of the spectrum of amplitudes. Experimental evidence showed the second set of descriptors was the most suitable to train the neural network to recognize with accuracy the presence and type of blockage. The obtained results compare favourably with the literature, indicating that the approach provides a tool to enhance process monitoring in water supply systems, in particular early detection of upstream blockages.

KEYWORDS

acoustic emission, neural network, online monitoring, pressure drop, turbulent flow

1 | INTRODUCTION

Effective control and monitoring systems are essential components for the maintenance of a reliable water distribution network. In this context, the early detection of partially blocked pipes and leakages is of particular importance. As the expense of providing clean water grows in many regions, the need to deploy effective and economical control systems is playing an increasing role in the sustainability of water distribution services. This need is likely to exacerbate in the near future, since projections assume a shortfall of 40% in water available to human use by as early as 2030.[1] By 2050 the United Nations Water Group estimates that two-thirds of the world population will suffer from water stress conditions.[2]

Moreover, in the manufacturing of liquid products, the development of smart sensors, capable of analyzing data gathered on pipe-lines and giving real time feedback, has been undergoing extensive research in the last years due to its potential benefits in terms of process optimization and more sustainable processes/products.[3] Innovation in this area often stems from technologies and methods developed in the fields of artificial intelligence and process engineering.[4]

Hefft and Alberini[5] investigated the use of machine learning to identify blockage type from pressure loss measurements in pipes, indicating that the approach can drastically help towards a better control of fluid flow delivery. Their pilot study included popular algorithms like decision trees,[6] k-nearest neighbours,[7] and support

vector machines (SVMs),[8] and the authors concluded that the latter delivered the best results.

The main limitation of SVMs is that they are only applicable to two-class problems. Hence, they can just identify one type of blockage against all other patterns. This work builds on the indications provided by Hefft and Alberini, tackling the problem of pipe obstruction identification from the perspective of pattern recognition. That is, the goal of the identification task is to recognize the presence and type of obstruction from patterns of acoustic emissions.

A popular artificial neural network (ANN) classifier, the multi-layer perceptron (MLP),[9] is used for the identification task. One of the main advantages of MLP with respect to SVM classifiers is that the former are suitable for multi-class problems. That is, they can be used to recognize different types of blockage. Inspired by the structure and functioning of biological nervous systems, the MLP has been widely employed because of its structural simplicity, fast learning capabilities, and ability to learn any categorical (classification) or continuous (regression) function with arbitrary precision.[10]

The article is organized as follows: Section 2 reviews current technology in the detection of water pipe blockages. Section 3 describes the proposed methodology and experimental set up. Section 4 presents the experimental results, which are discussed in Section 5. Section 6 concludes the paper.

2 | REVIEW OF CURRENT TECHNOLOGY

A very common tool to detect blockages in pipes is the tracing of pressure changes over the pipe length, as deposits or corrosion will consume pipe volume and lead to a pressure change.[11] The main limitation of this method is that it can only show the presence and size of the blockage, giving little information on its nature. This limitation is due to the mathematical formulation of the problem, which is commonly expressed using the Darcy-Weisbach relationship (applies to incompressible fluid flow only):

$$\Delta p_{v12}[Pa] = \frac{\rho \cdot u^2}{2}\left(\lambda \frac{l}{d} + \sum_i \xi_i\right) \tag{1}$$

where ρ is the density, u is the superficial velocity, λ is the Darcy friction factor, l is the length of pipe, d is the diameter, and ξ_i is the discharge coefficient.

The Darcy-Weisbach relationship can be extended to take the elevation and gravitational acceleration into account. This is achieved by applying the Bernoulli principle:

$$\Delta p_{v12}[Pa] = p_1 - p_2 + \frac{\rho}{2}\left(u_1^2 - u_2^2\right) + \rho \cdot g(h_1 - h_2) \tag{2}$$

where h are the elevations in the two different points where the pressure drop is measured. This Bernoulli extension is of particular importance for vertical pipe assemblies, such as those present in water wells, where the pressure drop is predominantly driven by the differences in elevation and not the frictional factor. In the oil and gas industry, horizontal wells are common, and it becomes important to have a better understanding of the frictional forces driving the pressure drop.[12] Other areas where a pressure drop measurement is standard routine are the prediction of membrane failure due to fouling[13] and process safety monitoring in parts such as a Venturi scrubber.[14] To determine the Darcy friction factor λ, empirical models depending on the flow regime are often applied. For laminar flow, the Hagen–Poiseuille equation states the following:

$$\lambda_{laminar} = \frac{64}{Re} \tag{3}$$

Moving into transient flow of the relationship as described in Colebrook and White[15] will qualify the following:

$$\frac{1}{\sqrt{\lambda}} = -2\log_{10}\left(\frac{2.51}{Re\sqrt{\lambda}} + \frac{k}{3.71d}\right) \tag{4}$$

where k is the Darcy-Weisbach Roughness height.

For flow approaching $Re \to \infty$ (hydraulic rough pipe wall) this model turns into the Nikuradse's relationship,[16] and when $k/d \to 0$ is reached (hydraulic smooth pipe), it turns into the Prandtl-Kármán's relationship.[17]

A review paper[18] compared different methodologies available to correlate the pressure drop to the friction factor, in order to find the most suitable method to replace the numerical root finding-based Colebrook–White relationship. The authors conclude that the Colebrook–White relationship can be best approximated using the method presented in this work.[19]

A study to investigate the pressure drop in helicoidally arranged pipes for single- and multi-phase systems was presented.[20] Other geometries that were studied include rectangular pipes[21] and polygons.[22] There are two standard approaches to measure the pressure drop in industrial settings.

The first method is the application of two independent pressure gauges (Figure 1A), mounted into the inlet and the outlet of the pipe system. As for most measurement systems, it can be implemented using analogue or digital devices. To avoid cross-contamination the devices often take the pressure readings through the displacement of a diaphragm. The pressure difference is

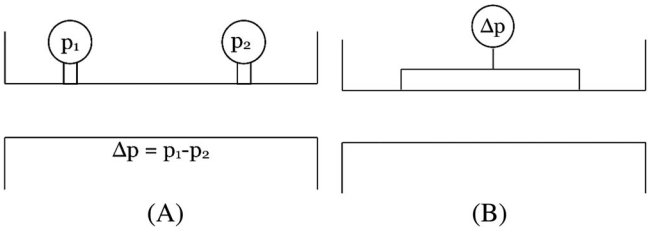

FIGURE 1 Basic principles to determine the pressure drop in a pipe. Schematic (A) shows a system based on two independent pressure gauges. Schematic (B) shows a system of a single gauge determining the pressure drop via capillaries

determined by the difference in readings between the two gauges.

The second method is based on a singular gauge (Figure 1B). Capillaries are connected to the pipe inlet and outlet, and determine the pressure drop based on the Bernoulli relationship.

An alternative approach has been investigated by Hefft and Alberini,[5] who obtained additional information on the type of geometry obstructing a pipe combining passive acoustic emission (AE) sensing with supervised machine learning. The sensitivity and accuracy of this approach is high, as the technique is capable of distinguishing between different obstructions under fully developed turbulent flow, where pressure drop measurements show no or only marginal differences in readings.

AEs are those events occurring past the audible spectrum (20 kHz) and before the ultrasound spectrum (2 MHz). AEs originate from elastic stresses or pressure waves that express themselves by dynamic surface motions. In the case of fluid flow, the boundary shear along the boundary layer causes AEs.[23]

There are two main drivers for the release of AEs. The first driver is the sudden and spontaneous release of transient energy when brittle material failure occurs (i.e., material fatigue or poor weld seams). The monitoring of these sudden energy releases is often used to ensure the structural integrity of bridges[24,25] or railways,[26,27] where material failure may have catastrophic consequences.

The second driver is material damage, which generates continuous AEs, and plays a key role in the field of tribology and hydrodynamics. Unlike the sudden release of transient energy in a single event, continuous AEs can be measured constantly. The monitoring of this second type of AEs is important to assess the wear of parts due to friction or impact,[28] or the presence of pipe leakages.[29,30] It is much more complex than monitoring single AE events, since the signals are noise-rich and of complex composition.[31]

AEs can be measured using active or passive sensing methods. Active AE sensing systems incorporate at least one signal emitter and a signal receiver. The whole technology is based on the idea of assessing the signal decay or damping between the emitter and receiver. This can be directly correlated to the leak location and size, and is often paired with differential pressure measurements.[32]

Passive AE sensing consists of a group of non-destructive testing systems that detect only the process/material-borne transient energy release. Unlike active technologies, passive AE measurements do not interfere with the fluid and material and only capture the events that are released by the system of interest. However, this technology is much less understood and studied compared to active AE techniques (e.g., compare Google Scholar 1:3 ratio of 347 search results for 'passive AE' versus 1060 results for 'active AE').

3 | MATERIALS AND METHODS

This section describes how the data was experimentally acquired and then processed. As shown in Figure 2, the key research steps are summarized and presented. Firstly, the data were collected using the experimental rig described in Section 3.1. Then, the data were converted from time domain to frequency domain. The next step was the extraction of descriptors (features). Two strategies are described and discussed. Finally, those descriptors are fed to the ANN and results are discussed.

3.1 | Experimental rig

A water recirculation system, previously used by Hefft and Alberini,[5] was fed by a 40-L water tank (A) and powered by a centrifugal pump (C) (Alfa Laval, Lund, Skåne, Sweden) of type I KA-5 132SSS1 controlled by an inverter (B). The internal diameter (ID) of the pipework was 25.4 mm with a 120-mm length pipe segment from stainless steel named Rheality pipe (E) (more information can be found at rheality.co), which was used for the acquisition of passive acoustic signals. A schematic drawing of the test rig and pipe inserts are shown in Figure 3.

Different types of obstruction and hence pressure drops (D) were simulated slotting into the pipe objects of different shapes (F1, F2, F3, F4). For each object, the AEs were measured at four different water flow rates using a Coriolis flow meter (G): 1300 (henceforth Q10), 3000 (henceforth Q20), 4530 (henceforth Q30), and 6350 (henceforth Q40) l h^{-1}. The nomenclature Q10, Q20, Q30, and Q40 comes from the settings of the pump used to generate the flow rates, which corresponds to 10, 20,

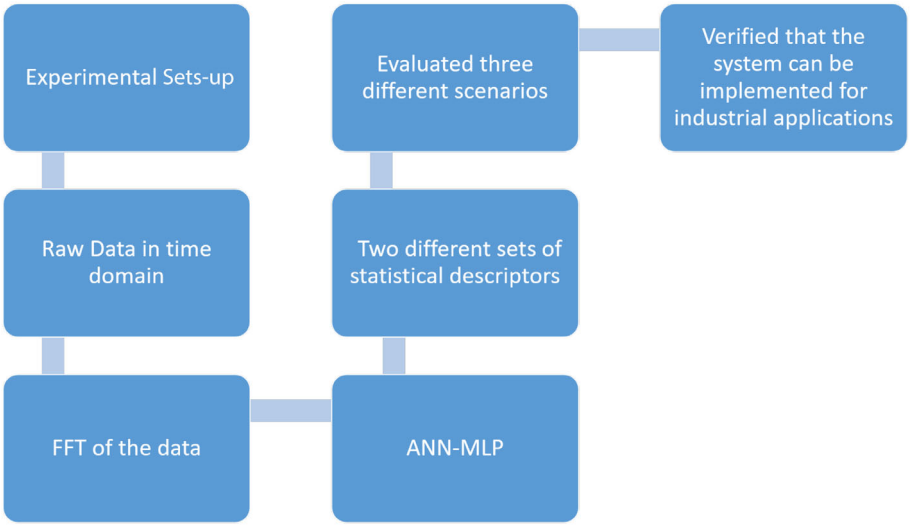

FIGURE 2 Block diagram of research steps

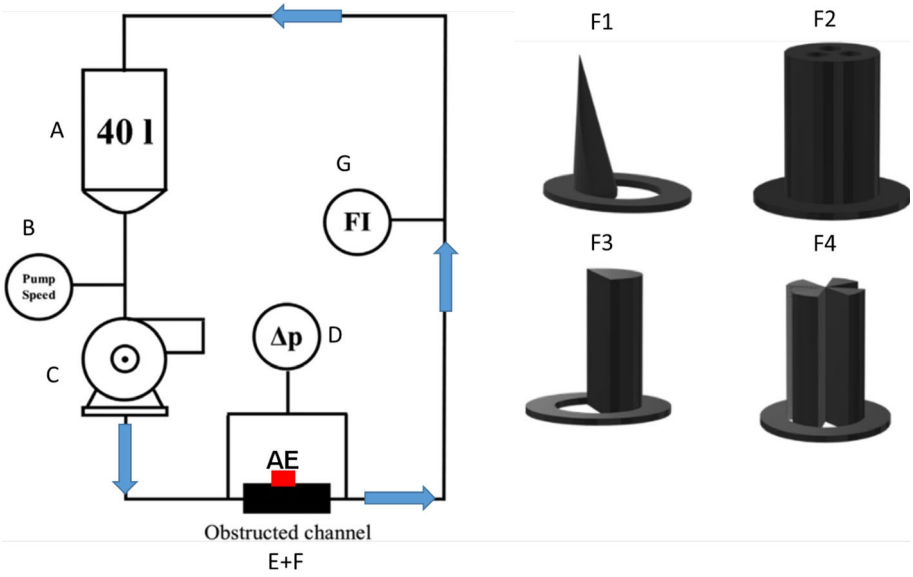

FIGURE 3 Test rig and obstruction shapes

30, and 40 Hz, respectively. The objects (F1, F2, F3, F4) were created using a FlashForge Dreamer 3D printer (Zhejiang Flashforge 3D Technology Co., Ltd., Jinhua, Zhejiang, China), and had a length (38.1 mm) equal to 1.5 times their inner diameter (25.4 mm). They are a wall-leaning cone (Cone), mimicking a slight build-up of deposit; a semicircle (Semicircle), mimicking a half blocked pipe; three triangular aligned holes (Holes), mimicking a full blockage with perforations delivering partial flow; and a cross (Cross) formed by four wedges meeting in the central focal point, mimicking the potential design of a spray nozzle. These four objects are shown in Figure 3. They had a free area of $1.287 \cdot 10^{-4} m^2$ (Cone), $2.53 \cdot 10^{-4} m^2$ (Semicircle), $2.83 \cdot 10^{-5} m^2$ (Holes), and $2.53 \cdot 10^{-4} m^2$ (Cross), respectively. A fifth case was considered where no insert was present and the pipe was free (Empty).

The goal of the study was to use ANNs to identify the presence and shape of the insert from the AE recording. The aim is to identify to which class (Cone, Cross, Hole, Semicircle, Empty) of pattern a passive acoustic recording belongs to.

The AE patterns were read using a piezoelectric VS375-M (Vallen Systeme GmbH, Icking, Bavaria, Germany) passive AE sensor. The sensor was coupled with the Rheality device (Rheality Ltd.) which allowed the detection of the signal in the fully flooded pipe, and linked to an AEP5H preamplifier (Vallen Systeme GmbH, Germany), along with a DCPL2 decoupling unit (Vallen Systeme GmbH, Icking, Bavaria, Germany), a PicoScope 5000 Series oscilloscope (Pico Technology Ltd., UK), and a personal computer using PicoScope version 6.13.15 software (Pico Technology Ltd., UK).

For each of the five types of obstructing objects (Cone, Cross, Hole, Semicircle, and Empty) and four flow rates (Q10-Q40), 200 AE recordings were performed. The whole experimental dataset is thus composed of 4000 AE patterns (200 recordings $\times 5$ types of objects $\times 4$ flow rates). Each recording is composed of 589 623 piezoelectric sensor readings, sampled at a frequency of 1.2 MHz and resolution of 16-bit for a total recording time of $\sim$0.5 s. The amplitude of the readings was clamped within ± 1 V and out-of-range readings (positive and negative) were converted to the minimum and maximum of the in-range readings. The dataset is freely available from the Mendeley Data repository by Baronti et al.[33]

3.2 | Data pre-processing

For each recording, the series of 589 623 piezoelectric sensor readings was converted from the time domain to the frequency domain using discrete fast Fourier transform (DFFT)[34] at a sampling rate of 694 444 Hz. Figure 4 shows the spectrum of average (median) DFFT amplitudes calculated over the 200 recordings for four types of obstruction (classes) for each flow rate. The spectra are shown in two ranges of frequencies where inter-class differences are particularly pronounced. The spectra of the Holes class are not shown as they are very dissimilar in magnitude from the other classes. Figure 4 suggests that the presence and type of obstruction can be identified from the different DFFT spectra, particularly at the highest flow rates.

The complete spectra for all the five classes until 130 kHz are provided in Appendix B. Beyond the 130 kHz of frequency the spectra flatten out, and to reduce computational overheads were not used. Henceforth, the AE patterns will be considered in the interval [0,130] kHz in the frequency domain.

3.3 | Feature extraction

In order to train an MLP classifier to recognize the different types of obstruction, some numerical descriptors (features) that capture the differences in DFFT spectra are needed. Two different sets of descriptors are evaluated in this study.

The first set (henceforth called AV) includes the average (mean) and variance over the 130 000 frequencies of the DFFT amplitude. This minimal set (only two) of well-understood statistical descriptors is conceptually simple and light in terms of processor and memory overheads. Yet, the scatter plots in Figures 5 and 6 show that, particularly at the highest flow rate, the readings are reasonably well clustered in the two-dimensional plane of the features.

The second set of features (henceforth called DB) is generated via data binning, dividing the spectrum into non-overlapping intervals of 100 frequencies, and taking the average (median) DFFT amplitude of the frequencies inside the interval as representative of the whole interval. The size of the bins was experimentally optimized, taking into account the trade-off between data compression and information loss. This second method creates a rather large set of features (130 000 *frequencies* $\div 100$ *bin size* $= 1300$ *features*), but retains more information about the DFFT spectrum than the AV set.

Thus, for each pattern, two feature sets are created, AV (2 elements) and DB (1300 elements), and each of the two sets is labelled with the class name (Cone, Cross, Hole, Semicircle, Empty) describing the type of insert that generated it. The mean–variance procedure[35] was subsequently used to normalize the feature values of each set within the $[-1,1]$ interval (except for outliers of feature values outside three standard deviations from the mean).

3.4 | MLP classifier

The MLP is arguably to date the most popular and widely used ANN model. It was chosen for this study because it is a universal approximator, capable of modelling the continuous or categorical output of any nonlinear function to an arbitrary degree of precision.

An MLP is composed of layers of simple non-linear processing nodes, called perceptrons (Figure 7). Each perceptron is fully connected to the nodes of the previous and next layer, except for those of the input layer (collecting the input pattern) and those of the output layer (giving the classification result). The strength (weight) of the connections between the nodes is adjustable. By changing these weights, the behaviour of the MLP can be modified (trained) to obtain the desired output. The signal flows unidirectionally layer-by-layer from the input to the output layer (feedforward ANN).

The input layer is composed of a number of nodes equal to the number of input features. Each unit takes one input variable (feature) and fans its value out to the nodes of the next layer. There are typically one or two layers of processing units between the input and output layer. These layers are called the hidden layers, and they are where the decision regions for the classification task are formed. It was shown that two layers of hidden units are enough to solve any arbitrarily complex identification problem.[36] The exact number of hidden layers and nodes per layer depends on the problem domain, and has

FIGURE 4 Spectra of average (median) of the DFFT amplitudes obtained in the 200 experimental tests, one plot per flow rate. The spectra are displayed in two frequency ranges where the differences are particularly marked. The spectra of the Holes class have been omitted because they are too different in magnitude (see Appendix B)

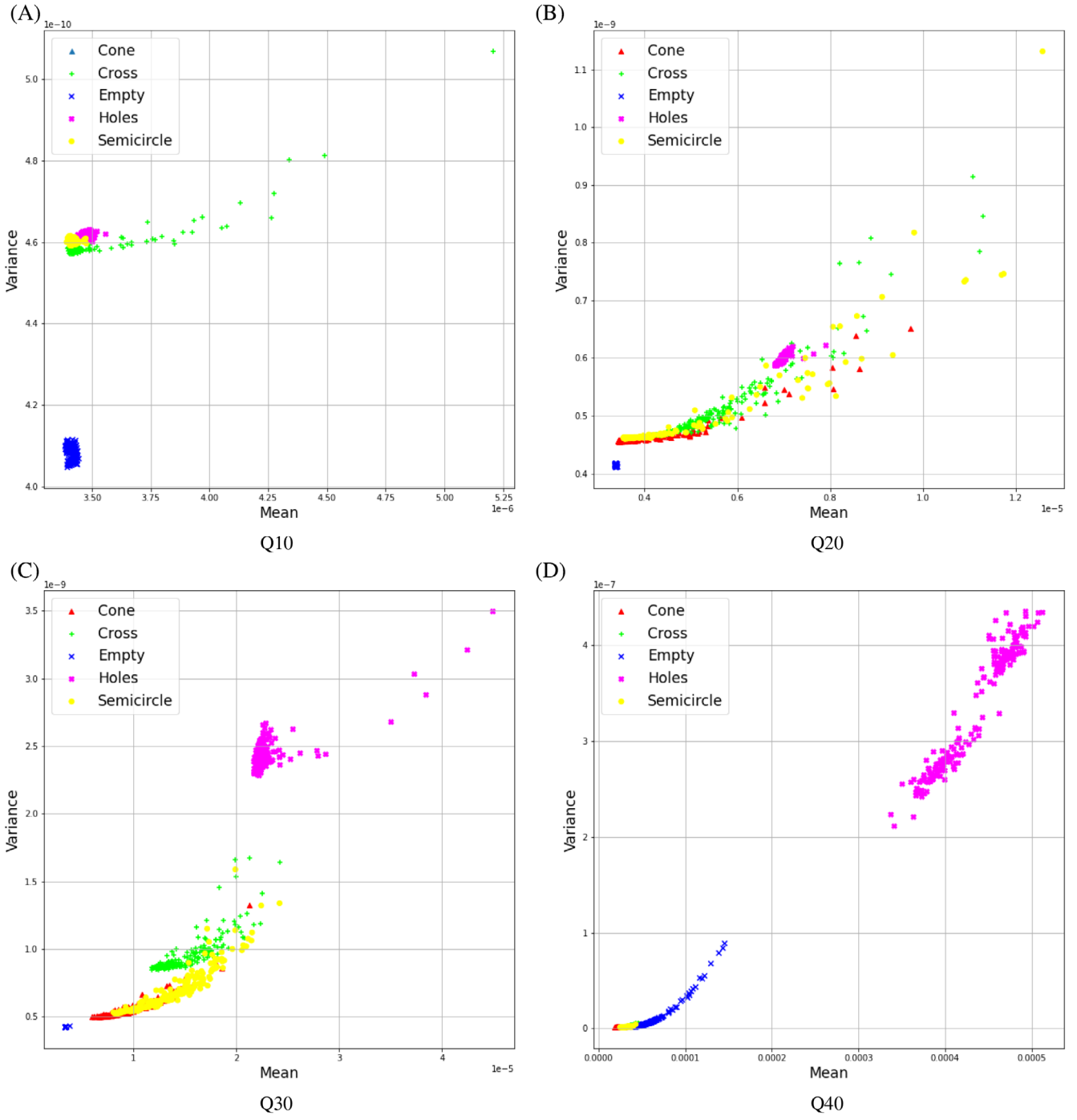

FIGURE 5 Plots of the distribution of the data patterns in the 2D space of the AV feature set. Each plot shows the distribution at a different flow rate, namely (A) Q10, (B) Q20, (C) Q30, and (D) Q40

been the topic of many studies.[37] Further hidden layers of processing nodes might be added to perform some pre-processing of the signal (e.g., data compression), and in this case the ANN structure is called deep.[38] The output layer contains one neuron per class, each neuron being associated with a particular class. Typically, the classification result is decided by the output node giving the highest numerical output.

The MLP training algorithm assumes an omniscient teacher who feeds the ANN the patterns of input features, and for each pattern indicates the expected output. The weights of the node connections are modified according to the error between the MLP actual and expected output. The most common training algorithms are iterative weight adjustment procedures based on least mean squares minimization of the ANN error. For more

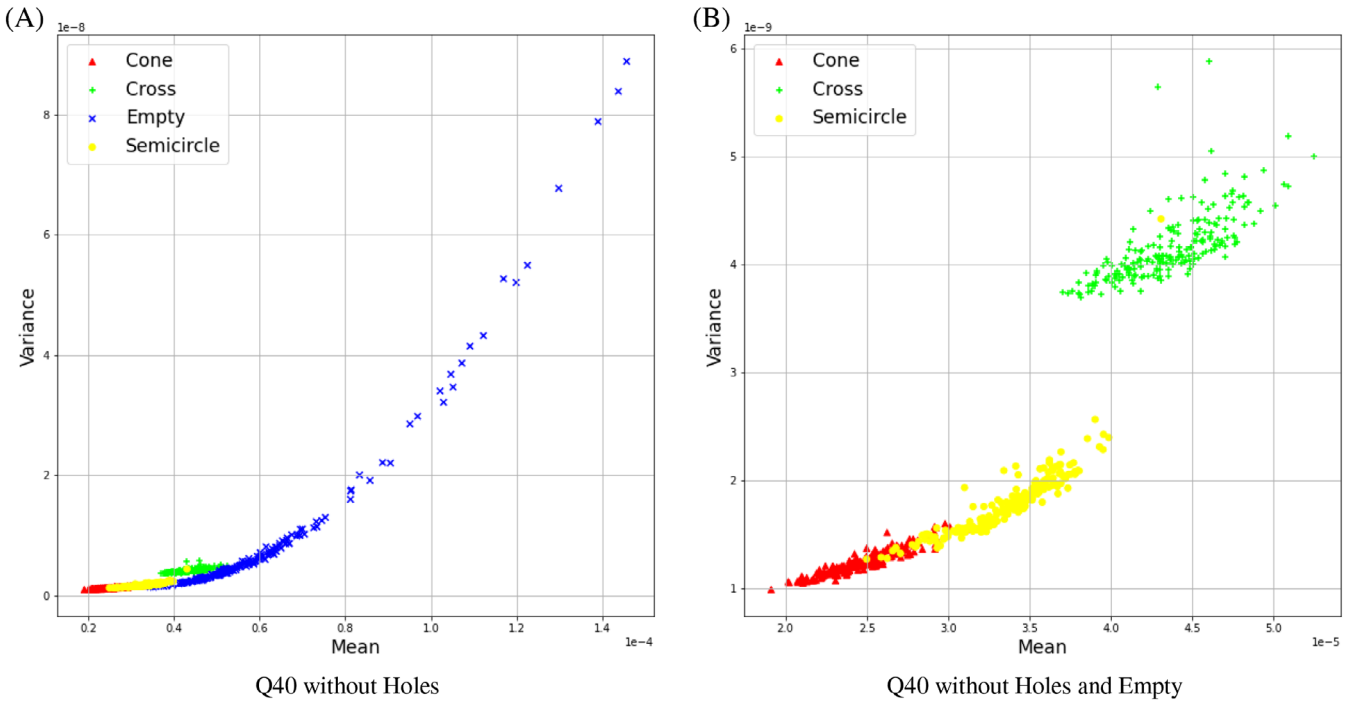

FIGURE 6 Plots of the distribution of the data patterns in the 2D space of the AV feature set at Q40 flow rate (Figure 5D) when the (A) Hole and (B) Hole and Empty classes are removed

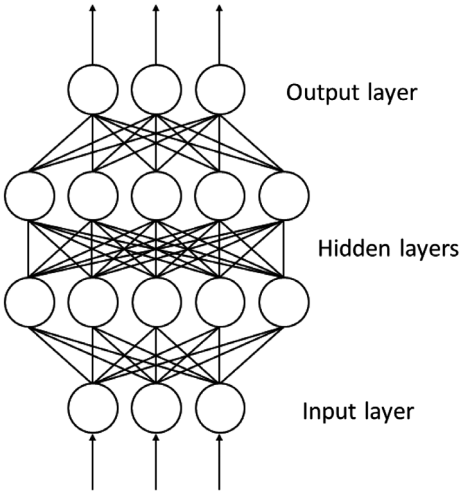

FIGURE 7 Example of general multi-layer perceptron (MLP) structure

TABLE 1 Models architecture

	MLP (AV)	MLP (DB)
Input size	2	1300
Hidden layer size	15	
Activation function (hidden)	ReLu	
Output layer size	5	
Activation function (output)	Softmax	
Loss function	Categorial crossentropy	
Optimizer	Adam	
Learning rate	0.01	
Number of epochs	5000	

details on the MLP, its processing units, and the training procedure, the reader is referred to the reviews of Lippmann[36] and Pham et al.[9]

Two MLPs were used in this study, one trained to classify the patterns characterized by the AV feature set, the other trained to classify the patterns characterized by the DB feature set. Their architecture was experimentally optimized, and is detailed in Table 1. In both cases, the size of the input layer was determined by the feature set used: 2 units for the MLP using the AV set, and 1300 units for the MLP using the DB set. Regardless of the feature set used, the best results were obtained using MLPs featuring one hidden layer of 15 units. The output layer was composed of five nodes, one per class.

The two ANNs were trained using the state-of-the-art ADAM optimizer,[39] (please note that Kingma and Ba[39] is from a conference, and the preprint is available in the popular open access arXiv repository) using the standard categorical cross-entropy loss function.[40] For each pattern, the cross-entropy objective function is defined as follows:

TABLE 2 Five-value summary of the accuracy results obtained in the 100 independent learning trials using the AV feature set (the rows indicated with T report the accuracy results obtained from the training sets of examples, whilst the rows indicated with V report the accuracy results obtained from the validation sets of examples)

Rate		Min	First quartile	Median	Third quartile	Max
Q10	T	0.6129	0.7571	0.7743	0.7814	0.8057
	V	0.6033	0.7500	0.7700	0.7867	0.8133
Q20	T	0.7143	0.7571	0.7671	0.7757	0.8043
	V	0.6900	0.7533	0.7667	0.800	0.8533
Q30	T	0.6757	0.7314	0.7371	0.7429	0.7557
	V	0.6533	0.7200	0.7400	0.7467	0.7667
Q40	T	0.8729	0.8943	0.9000	0.9057	0.9171
	V	0.8500	0.8867	0.8967	0.9067	0.9300

$$L(o,y) = -\sum_{i=0}^{4} y_i \log_e(o_i) \tag{5}$$

where o is the ANN output vector and y is the target vector. The target vector y is composed of five elements, one per class. It is one-hot encoded, namely, all its elements are zero but the one associated with the correct class, which is equal to 1. The vector o is composed of five elements, each one representing the output of a different output neuron. Since the output units use the softmax function, the elements o_i are defined in the $[0,1]$ range, and o is normalized to 1. It should be noted that the only non-zero element of y that contributes to the sum in Equation (5) is the one associated to the correct class. The sum will be minimum when the output of the neuron associated to the target class is equal to 1, that is, $o_t = y_t = 1$, and consequently the output of all the other neurons, $o_j = 0$, $j \neq k$. The ADAM optimizer uses gradient descent to minimize $L(o,y)$.

4 | EXPERIMENTAL RESULTS

The aim of this study was to assess the ability of the MLP to learn to identify the presence and type of obstruction from the patterns of AEs. As discussed in Section 3, two data sets were created, the first using the set of AV features to characterize the individual patterns, the second using the set of DB features. These two data sets were used to train two different MLPs. Three experiments were carried out.

In the first experiment, the two MLPs were trained to identify the patterns at a fixed flow rate. Thus, for each flow rate (Q10–Q40), the 1000 patterns $(200\ \textit{recordings} \times 5\ \textit{types of objects})$ were randomly split into a training set of examples including 70% of the patterns and a validation set including the remaining 30%. The MLP was trained on the former and the latter was used to test the learning results. The split was done using a stratified sampling, meaning that 30% of the patterns belonging to each class was picked to form the test set. Hence, the training and test set had a balanced number of examples per class. The separation of the data set was necessary to verify that the MLP is able to generalize the training results to unseen data samples, or, in statistical jargon, that the evaluation of the training results is unbiased.[41]

For each flow rate, 100 independent learning trials were performed, each time randomly re-initializing the MLP connection weights and the training and validation sets of examples. The classification accuracies obtained by the trained MLP in the 100 learning trials are summarized in Table 2 (AV set of features) and Table 3 (DB set of features). The two tables show that in all cases but Q10 in Table 4, the difference between training and test accuracy is negligible. This suggests there was no data overfitting.

The experimental results show that, at fixed flow rate, the MLP can be consistently trained to recognize with high accuracy the AE patterns using the DB feature set. Except for the lowest flow rate, the classification accuracy in nearly all the learning trials was very close or equal to 1. The MLPs were able to generalize the learning results to the previously unseen patterns of the validation set with very small or no loss of accuracy, indicating the reliability of the training procedure.

The learning results obtained using the AV feature set were satisfactory only at the highest flow rate. Yet, at lower flow rates, the MLP could still be trained to recognize three quarters of the AE patterns successfully. In general, the results of Table 2 confirm that the patterns tend to cluster more clearly (and hence are easier to distinguish) at high flow rate (Figure 5).

To analyze the sources of errors, the first experiment was repeated for the patterns generated at flow rate Q40 using the AV feature set, and the confusion matrix was formed considering the errors on the whole data set (training + validation set). Looking at Table 4, it is apparent that the main sources of misclassification concerned the pairs of classes Cone-Semicircle, Cross-Semicircle,

Rate		Min	First quartile	Median	Third quartile	Max
Q10	T	1:000	1:000	1:000	1:000	1:000
	V	0:7900	0:8433	0:8600	0:8733	0:9000
Q20	T	1:000	1:000	1:000	1:000	1:000
	V	0:9833	0:9933	0:9967	1:000	1:000
Q30	T	1:000	1:000	1:000	1:000	1:000
	V	0:9967	1:000	1:000	1:000	1:000
Q40	T	1:000	1:000	1:000	1:000	1:000
	V	0:9967	1:000	1:000	1:000	1:000

TABLE 3 Five-value summary of the accuracy results obtained in the 100 independent learning trials using the DB feature set (the rows indicated with T report the accuracy results obtained from the training sets of examples, whilst the rows indicated with V report the accuracy results obtained from the validation sets of examples)

		Actual				
		Cone	Cross	Empty	Holes	Semicircle
Predicted	Cone	180.62	2	0	0	17.38
	Cross	0	177.18	12.75	0	10.07
	Empty	0	26.59	172.62	0.04	0.75
	Holes	0	2.0	0	198.0	0
	Semicircle	18.82	16.39	0	0	164.79

TABLE 4 Confusion matrix (predicted class vs. actual class) of the performance of the multi-layer perceptron (MLP) on the patterns (training + validation set) generated using feature set AV at flow rate Q40

TABLE 5 Accuracy results obtained training the multi-layer-perceptrons (MLPs) on patterns obtained at a given flow rate, and testing them on patterns generated at a different flow rate (AV feature set); for each flow rate, the MLP that obtained the best training accuracy in the experiment summarized in Table 2 was used, and the learning results were validated on the whole (training + validation) data sets

Test				
Training	Q10	Q20	Q30	Q40
Q10	0:786	0:204	0:200	0:200
Q20	0:200	0:843	0:200	0:200
Q30	0:200	0:200	0:740	0:200
Q40	0:287	0:197	0:203	0:903

TABLE 6 Accuracy results obtained from training the multi-layer-perceptrons (MLPs) on patterns obtained at a given flow rate, and testing them on patterns generated at a different flow rate (DB feature set); for each flow rate, the MLP that obtained the best training accuracy in the experiment summarized in Table 3 was used and the learning results were validated on the whole (training + validation) data sets

Test				
Training	Q10	Q20	Q30	Q40
Q10	0:9700	0:4380	0:2050	0:2940
Q20	0:4150	1:000	0:9990	0:3980
Q30	0:4210	0:7640	1:000	0:4140
Q40	0:2390	0:4050	0:5660	1:000

and Cross-Empty, which look very close or overlap in the AV feature space in Figures 5 and 6. Conversely, the patterns of the Holes class constitute a very distinct cluster in Figure 5, and are identified without error by the MLP.

In the second experiment, it was verified whether the training results obtained at a given flow rate were transferable to patterns acquired at a different flow rate. The experiment was set as follows. For each flow rate, the most successful learning trial was decided as the one where the highest classification accuracy was obtained from the validation set of examples (Tables 2 and 3). The trained MLP configuration obtained during the most successful learning trial was then tested against the patterns generated at the other three flow rates. In this case, all the patterns generated at a different flow rate had not been employed for training the MLP, and the MLP could be tested on the whole data set (training + validation set). For consistency, the MLP accuracy was also tested on the whole data set where it was trained. Although this latter measure was not guaranteed to be statistically unbiased, it was used to provide the reader a term for a quick qualitative comparison.

The results of this second experiment are presented in Table 5 for the patterns generated using the AV feature

TABLE 7 Five-value summary of the accuracy results obtained in 100 independent learning trials by the multi-layer perceptrons (MLPs) using the AV (first) and DB (second) feature sets (the patterns were used regardless of the flow rate at which they were generated; the rows indicated with T report the accuracy results obtained from the training sets of examples, whilst the rows indicated with V report the accuracy results obtained from the validation sets of examples)

Model		Min	First quartile	Median	Third quartile	Max
MLP (AV)	T	0:3071	0:4771	0:5357	0:6014	0:7186
MLP (AV)	V	0:3021	0:4558	0:5203	0:5845	0:6991
MLP (DB)	T	1:000	1:000	1:000	1:000	1:000
MLP (DB)	V	0:9127	0:9361	0:9412	0:9455	0:9555

set, and in Table 6 for the patterns generated using the DB feature set. The tables clearly show that the learning results obtained at a given flow rate are generally not transferable to patterns generated at different flow rates. The accuracy of the MLP trained using the AV feature set is equal to the null accuracy (accuracy that would be attained by random guessing) at a different flow rate. The learning results obtained at a given flow rate using the DB feature set are generally above the null accuracy at different flow rates, although they are generally far from being acceptable. Overall, the results of the second experiment are explained by the large differences in the arrangement of the data clusters between plots obtained at different flow rates (Figure 5).

In the third experiment, the AE patterns obtained at different flow rates were combined into one unique data set of 4000 elements (1000 per flow rate). This data set was split into a training set containing 70% of the patterns, and a validation set containing the remaining 30%. The split was done via stratified sampling, picking an equal number of samples for each class regardless of the flow rate at which they had been generated. The aim of this experiment was to investigate if data samples generated at different flow rates could be used to train the MLP to recognize AE patterns regardless of the flow rate. The results are detailed in Table 7, and show that the learning task could be performed satisfactorily only by the MLP trained using the DB feature set.

5 | DISCUSSION

This study built on the work by Hefft and Alberini,[5] further exploring the potentiality of machine learning to detect and identify the presence of blockage in pipes from AE patterns. The main advance in the proposed study is the replacement of the SVM classifier (only suitable for two-class problems) with an MLP classifier (suitable for multi-class problems). Other advantages of the MLP over SVMs are usually faster learning times and reduced memory requirements.

In terms of classification accuracy, Hefft and Alberini[5] reported results ranging between 96% to 97% for their binary classifiers (one obstruction type vs. all other cases) at fixed flow rates. In this scenario (Table 3), the MLP outperforms the SVM when the DB feature set is used. Using the DB feature set, the MLP achieves a classification accuracy of 94% even when patterns are mixed regardless of the flow rates (Table 6). In general, it can be said that the MLP approach is more accurate than the SVM.

The main sources of error (Table 4 and Figures 5 and 6) at fixed flow rate seem to originate from the nature of the data (some classes are overlapping in the feature space), rather than poor learning of the classifier. At different flow rates, the patterns cluster differently and seem to be less distinguishable at low flow rates. If the MLP is required to identify obstruction patterns at different flow rates, the training set of examples must cover the whole range of operational conditions.

It might be possible to extract data features that can help distinguish more clearly the clusters of AE patterns. In addition to the two sets of features evaluated in this study, Hefft and Alberini[5] used the 5000 DFFT amplitudes with the largest relative variance, picking from this set the largest 15 principal components. Their set was more complex than the AV (two features) and DB (1300 features) sets used in this study, although the precision of the trained classifier did not seem to benefit from the additional complexity.

The results achieved in this study show concrete developments towards a new smart sensor technology, which could have direct applications in the manufacturing pipelines of liquid products as well as wastewater and sludge treatments plants. This technology, a smart pressure drop reader, has been demonstrated to be a source of complex information which can be used for accurate process monitoring. As highlighted by Hefft and Alberini,[5] at present pressure drop measurements are limited to Δp readings. Unfortunately, similar readings may result from different causes within the process.

The novelty of this study is in the combination of off-the-shelf data techniques with a new application, passive acoustic sensor technology, for the monitoring of the pressure drop in pipes. In particular, Rheality is a new patented technology which enables such measurements. For the first time, acquired data were analyzed to determine the most valuable and descriptive features. The proposed new method provides information which can be unambiguously related to the type of blockage. This possibility is a game changer, which could lead towards a better control of undesired phenomena within the process line.

6 | CONCLUSIONS

Acoustic emission (AE) data were used to identify the presence and type of blockage from pressure loss measurements in pipes. The data were processed according to the following steps:

i. The AE measurements were pre-processed using Fourier analysis, and classified into blockage type using a popular artificial neural network (ANN), the multi-layer perceptron (MLP).
ii. Two different sets of statistical data descriptors were evaluated as input to the ANN. The first (AV) used the average and variance of the DFFT amplitudes over the 130 000 AE frequencies. The second set (DB) was generated via data binning, dividing the DFFT spectrum into non-overlapping intervals of 100 frequencies, and taking the average amplitude as the representative of each bin.

The following outcomes were achieved:

- The tests showed that, at fixed flow rate, the MLP can be consistently trained to identify with near perfect accuracy the AE patterns using the DB feature set. The learning results obtained using the AV feature set were satisfactory only at the highest flow rate. Yet, at lower flow rates, the MLP could still be trained to recognize three quarters of the AE patterns successfully.
- It was verified whether the training results obtained at a given flow rate were transferable to patterns acquired at a different flow rate. The results were negative, indicating that the AE patterns and their relative differences are strongly related to the flow rate.
- However, experimental evidence showed that, when trained using patterns generated at various flow rates, the MLP can be trained to recognize blockage types at any flow rate.

In summary, it can be concluded that the above results are encouraging, and the proposed system can be readily implemented in a real application for the monitoring of pressure drops in pipes. This smart tool can be used to provide precise information of what is happening inside the pipe, a task which is beyond the current state-of-the-art based on standard pressure drop measurements. This capability has important implications for online monitoring in industrial processes.

Further work should be carried out to investigate the suitability of the proposed data analysis approach to detect different features of the flow, which could include the presence of different phases (gas or solids) or even recognize different flow rates. Further work should also address the feature generation processes, in order to improve the MLP classification accuracy, possibly including deep learning techniques. In this latter case, the gains in accuracy should be evaluated against the increased complexity of the ANN structure and its training procedure.

PEER REVIEW

The peer review history for this article is available at https://publons.com/publon/10.1002/cjce.24202.

NOMENCLATURE

Acronyms

Hz	hertz ($1/s$)
AE	acoustic emission
ANN	artificial neural network
AV	average and variance
DB	data binning
DFFT	discrete fast Fourier transform
MLP	multi-layer perceptron
Re	Reynolds number
SVM	support-vector machine

Greek letters

Δp	pressure loss (Pa)
λ	Darcy friction factor (−)
ρ	density (kg/m^3)
ξ	discharge coefficient (−)

Roman letters

d	internal pipe diameter (m)
g	gravity (m/s^2)
h	elevation (m)
i	index (−)
k	Darcy-Weisbach roughness height (m)
l	length (m)
p	pressure (Pa)
u	superficial velocity (m/s)

ORCID

Federico Alberini https://orcid.org/0000-0001-8479-6330

REFERENCES

[1] V. Ayyam, S. Palanivel, S. Chandrakasan, in *Coastal Ecosystems of the Tropics-Adaptive Management* (Eds: V. Ayyam, S. Palanivel, S. Chandrakasan), Springer, Singapore **2019**, p. 153.
[2] Food and Agriculture Organization of the United Nations, *The State of Food and Agriculture*, Food and Agriculture Organization of the United Nations, Rome, Italy **2007**.
[3] V. Venkatasubramanian, *AIChE J.* **2019**, *65*, 466. https://doi.org/10.1002/aic.16489.
[4] S. J. Qin, L. H. Chiang, *Comput. Chem. Eng.* **2019**, *126*, 465.
[5] D. I. Hefft, F. Alberini, *Biosyst. Eng.* **2020**, *191*, 48.
[6] L. Rokach, O. Z. Maimon, *Data Mining with Decision Trees: Theory and Applications*, World Scientific, Singapore **2008**.
[7] N. S. Altman, *Am. Stat.* **1992**, *46*, 175.
[8] Z. Xuegong, *Acta Automatica Sinica* **2000**, *26*, 32.
[9] D. T. Pham, M. Packianather, A. Afify, in *Computational Intelligence* (Eds: D. Andina, D. T. Pham), Springer, Boston, MA **2007**, p. 67.
[10] K. Hornik, M. Stinchcombe, H. White, *Neural Networks* **1989**, *2*, 359.
[11] H. Liu, *Pipeline Engineering*, CRC Press, Boca Raton, FL **2003**.
[12] Z. Su, J. Gudmundsson, presented at the SPE Asia Pacific Oil and Gas Conf., Melbourne, Australia, November 1994.
[13] J. Vrouwenvelder, J. Kruithof, *Biofouling of Spiral Wound Membrane Systems*, Iwa Publishing, London, UK **2011**.
[14] B. Azzopardi, S. Teixeira, A. Govan, T. Bott, *Process Saf. Environ.* **1991**, *69*, 237.
[15] C. Colebrook, C. White, *P. Roy. Soc. Lond. A Mat.* **1937**, *161*, 367.
[16] J. Nikuradse, *Strömungsgesetze in rauhen Rohren*, VDIVerlag, Weinheim, Germany **1933**.
[17] P. Kurzweil, B. Frenzel, F. Gebhard, in *Physik Formelsammlung: Für Ingenieure und Naturwissenschaftler* (Ed: P. Kurzweil), Vieweg, Wiesbaden, Germany **2008**, p. 56.
[18] O. E. Turgut, M. Asker, M. T. Coban, *Bitlis Eren University Journal of Science and Technology* **2014**, *4*, 1.
[19] C. Goudar, J. Sonnad, *Hydrocarb. Process.* **2008**, *87*, 79.
[20] R. Xin, A. Awwad, Z. Dong, M. Ebadian, *Int. J. Heat Fluid Fl.* **1997**, *18*, 482.
[21] L. Guo, D. M. Chong-Fang, *J. Eng. Thermophys.* **2006**, *27*, 185.
[22] W. Y. Tey, H. S. Kang, *Progress in Energy and Environment* **2018**, *7*, 1.
[23] H. Hardy, F. W. Leighton, *Acoustic Emission-Microseismic Activity in Geologic Structures and Materials*, Trans Tech Publications, Limited, Zurich, Switzerland **1984**.
[24] A. Nair, C. Cai, *Eng. Struct.* **2010**, *32*, 1704.
[25] J. Yu, P. Ziehl, B. Zárate, J. Caicedo, *J. Constr. Steel Res.* **2011**, *67*, 1254.
[26] S. Shi, Z. Han, Z. Liu, P. Vallely, S. Soua, S. Kaewunruen, M. Papaelias, *P. I. Mech. Eng. F-J. Rai.* **2018**, *232*, 1211.
[27] J. Wang, X.-Z. Liu, Y.-Q. Ni, *Comput.-Aided Civ. Inf.* **2018**, *33*, 21.
[28] D. Mba, *Journal of Failure Analysis and Prevention* **2008**, *8*, 188.
[29] M. R. Lee, J. H. Lee, *Solid State Phenomena*, Trans Tech Publications, Zurich, Switzerland **2006**, p. 79.
[30] A. Mostafapour, S. Davoudi, *Appl. Acoust.* **2013**, *74*, 335.
[31] A. Glowacz, *Eksploat. Niezawodn.* **2015**, *17*, 64.
[32] J. W. Boyd, J. Varley, *Chem. Eng. Sci.* **2001**, *56*, 1749.
[33] Passive acoustic flooded pipe dataset, https://data.mendeley.com/datasets/5kjxpcwm69/1 (accessed: May 2021).
[34] J. C. Schatzman, *SIAM J. Sci. Comput.* **1996**, *17*, 1150.
[35] D. Freedman, R. Pisani, R. Purves, *Statistics*, Cambridge University Press, New York **1998**.
[36] R. Lippmann, *IEEE ASSP Magazine* **1987**, *4*, 4.
[37] M. Castellani, *Neurocomputing* **2013**, *99*, 214.
[38] Y. LeCun, Y. Bengio, G. Hinton, *Nature* **2015**, *521*, 436.
[39] D. P. Kingma, J. L. Ba, presented at the ICLR: Int. Conf. on Learning Representations, San Diego, CA, May 2015.
[40] K. P. Murphy, *Machine Learning: A Probabilistic Perspective*, MIT Press, Cambridge, MA **2012**.
[41] G. James, D. Witten, T. Hastie, R. Tibshirani, *An Introduction to Statistical Learning with Applications in R*, 6th ed., Springer, New York **2015**.

How to cite this article: L. Baronti, M. Castellani, D. Hefft, F. Alberini, *Can J Chem Eng* **2021**, 1. https://doi.org/10.1002/cjce.24202

APPENDIX A.: RHEALITY TECHNOLOGY

Figure A1 shows the Rheality system used to acquire the measurements.

FIGURE A1 Rheality system

APPENDIX B.: INTRA-CLASS AND INTER-CLASS DIFFERENCES

This appendix contains the complete spectra for all the five classes until 130 kHz. The plots in Figures B1 to B4 show the (column-wise) five-value summary of the 200 experiments for each shape and each flow rate. Figure B5 shows the spectrum of average (median) DFFT amplitudes calculated over the 200 recordings for the five types of obstruction (classes) for each flow rate.

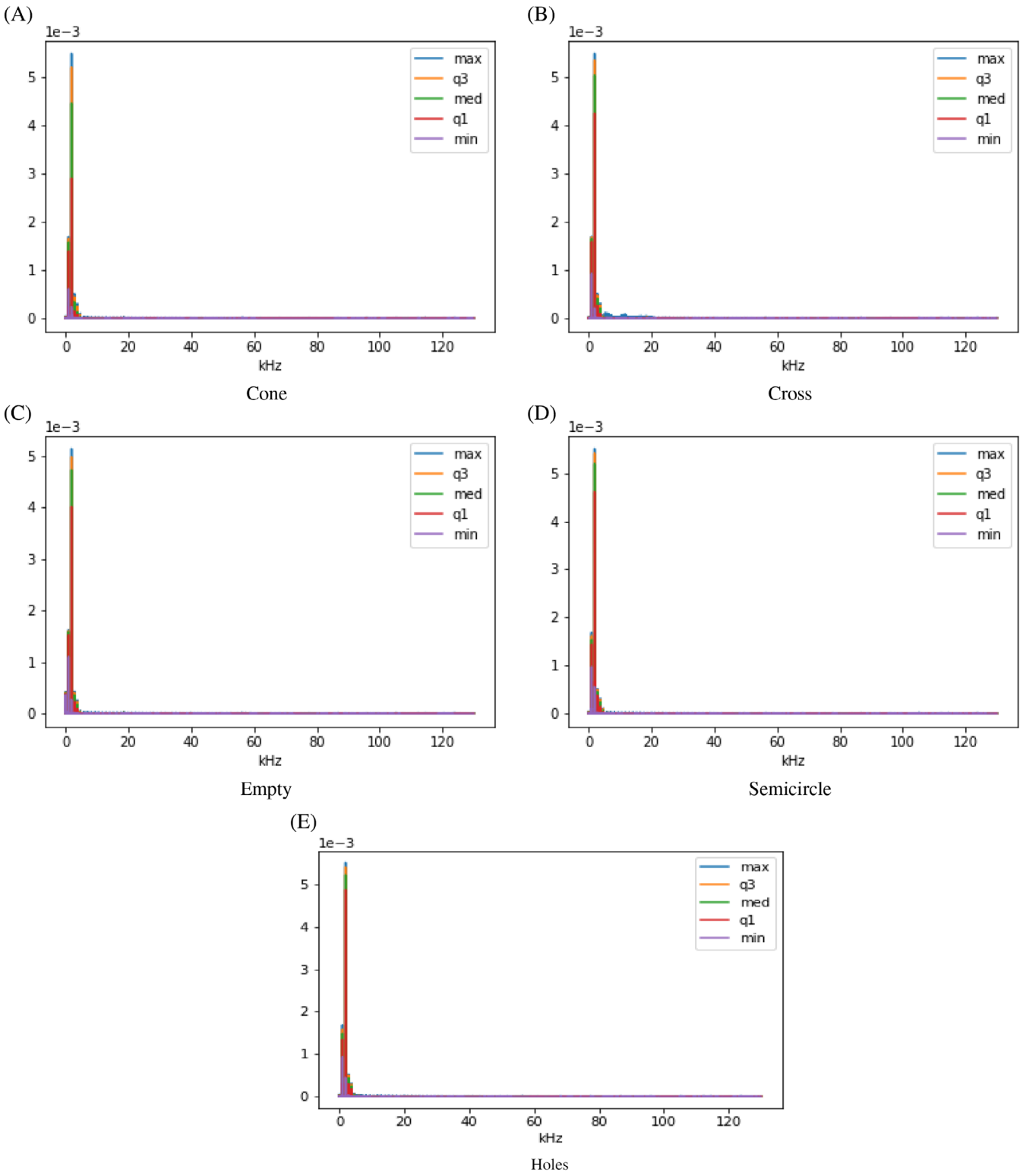

FIGURE B1 Intra-class difference, in the form of column-wise five-value summary, of the 200 experiments for each class at Q10 flow rate

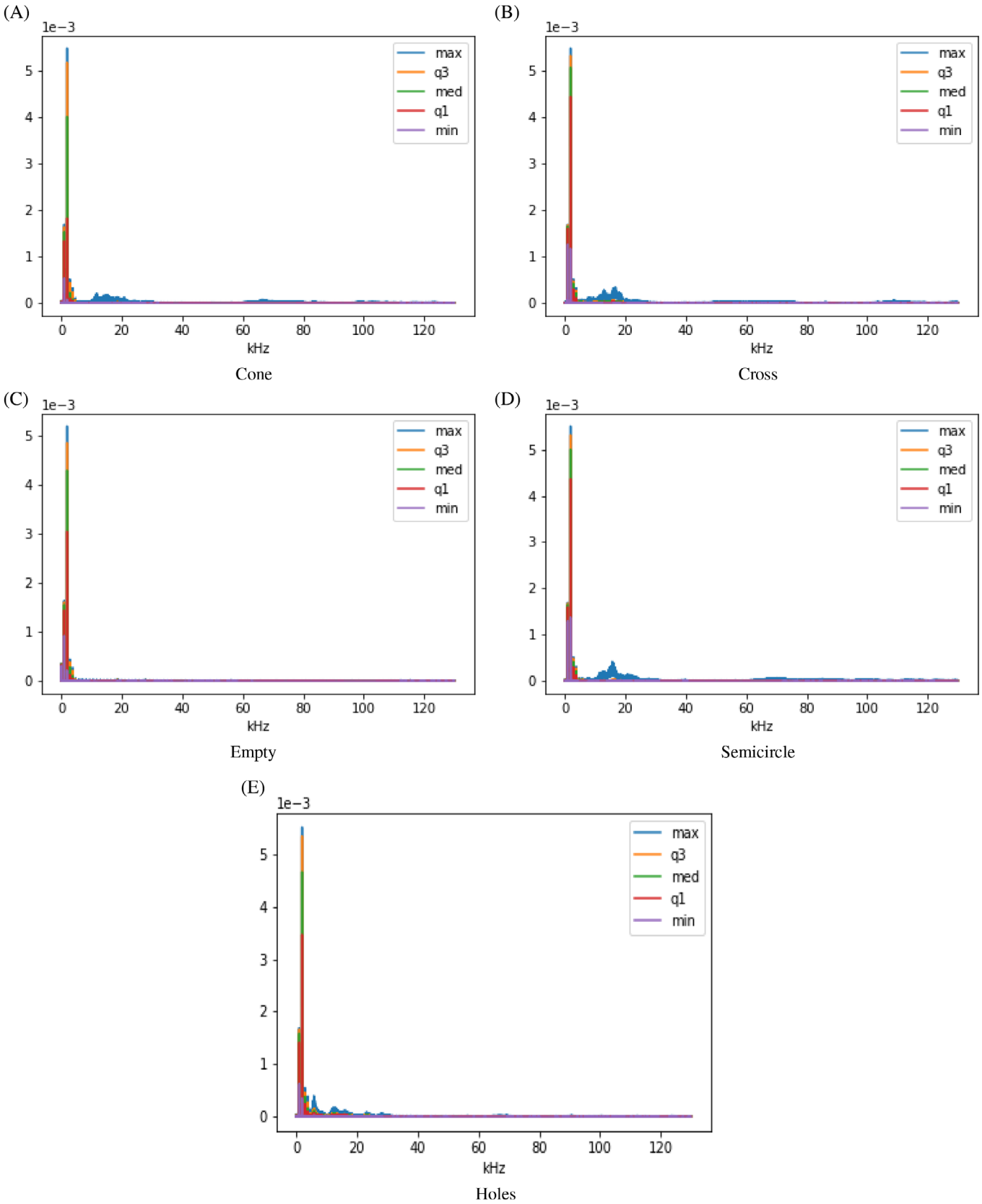

FIGURE B2 Intra-class difference, in the form of column-wise five-value summary, of the 200 experiments for each class at Q20 flow rate

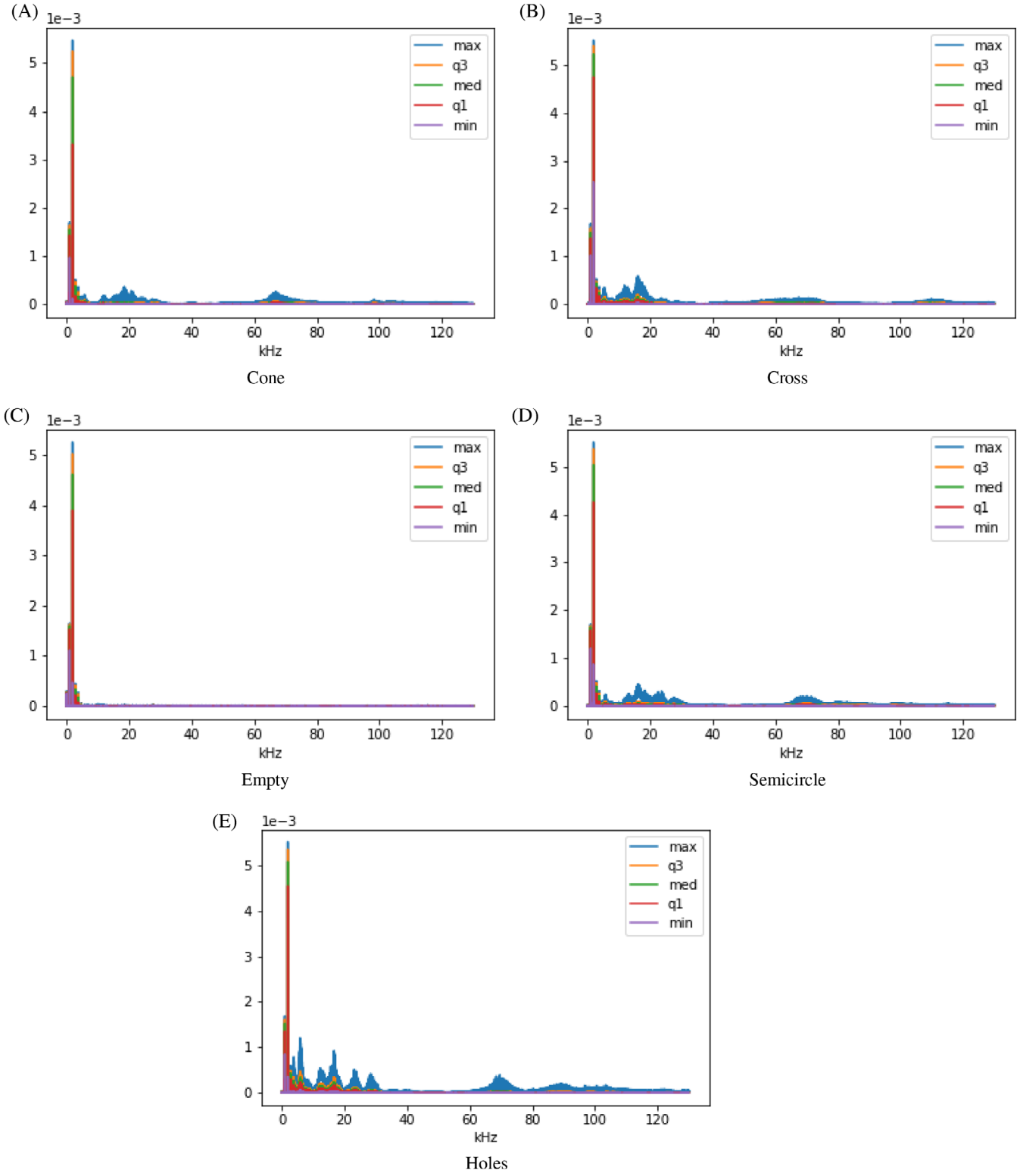

FIGURE B3 Intra-class difference, in the form of column-wise five-value summary, of the 200 experiments for each class at Q30 flow rate

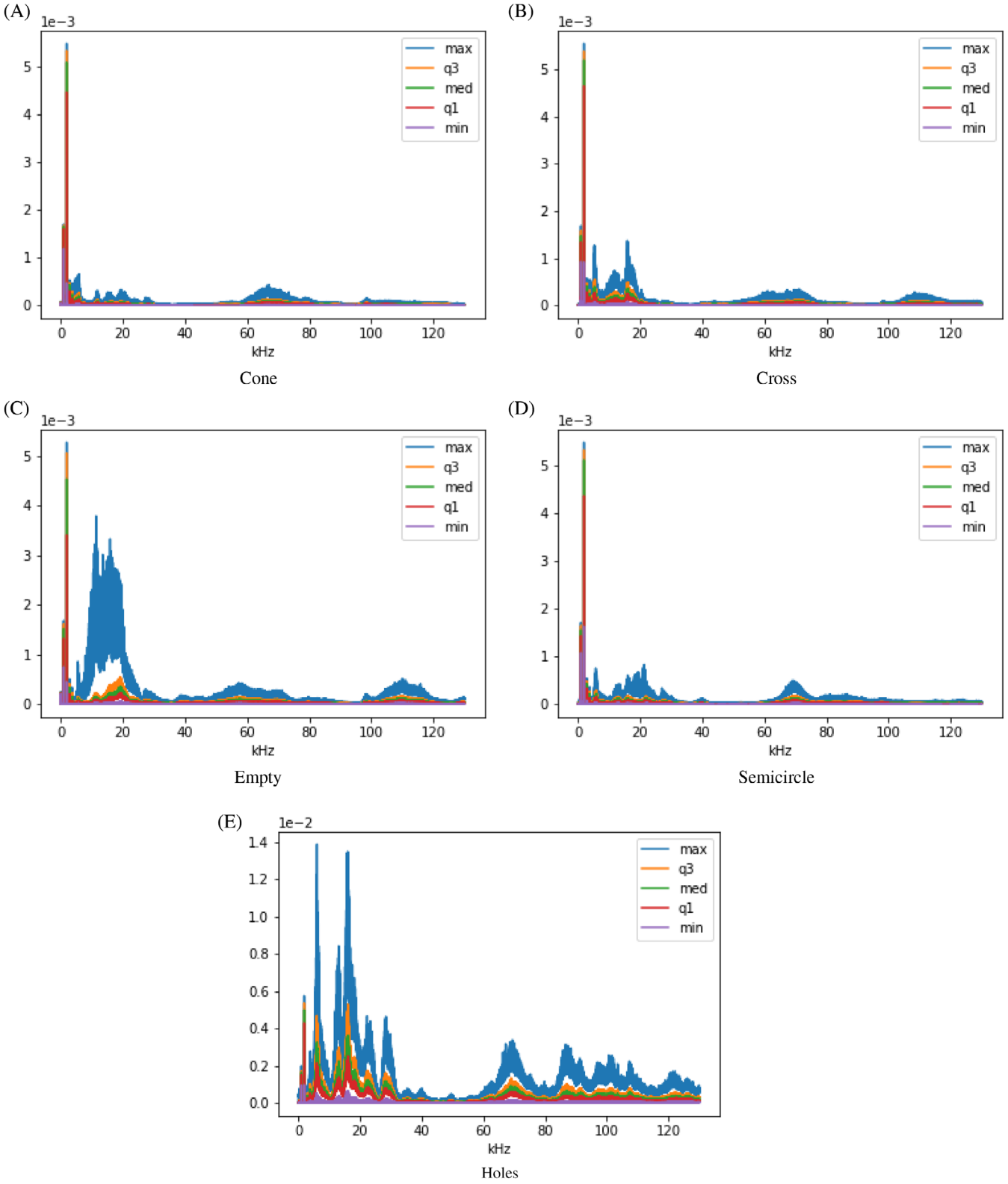

FIGURE B4 Intra-class difference, in the form of column-wise five-value summary, of the 200 experiments for each class at Q40 flow rate

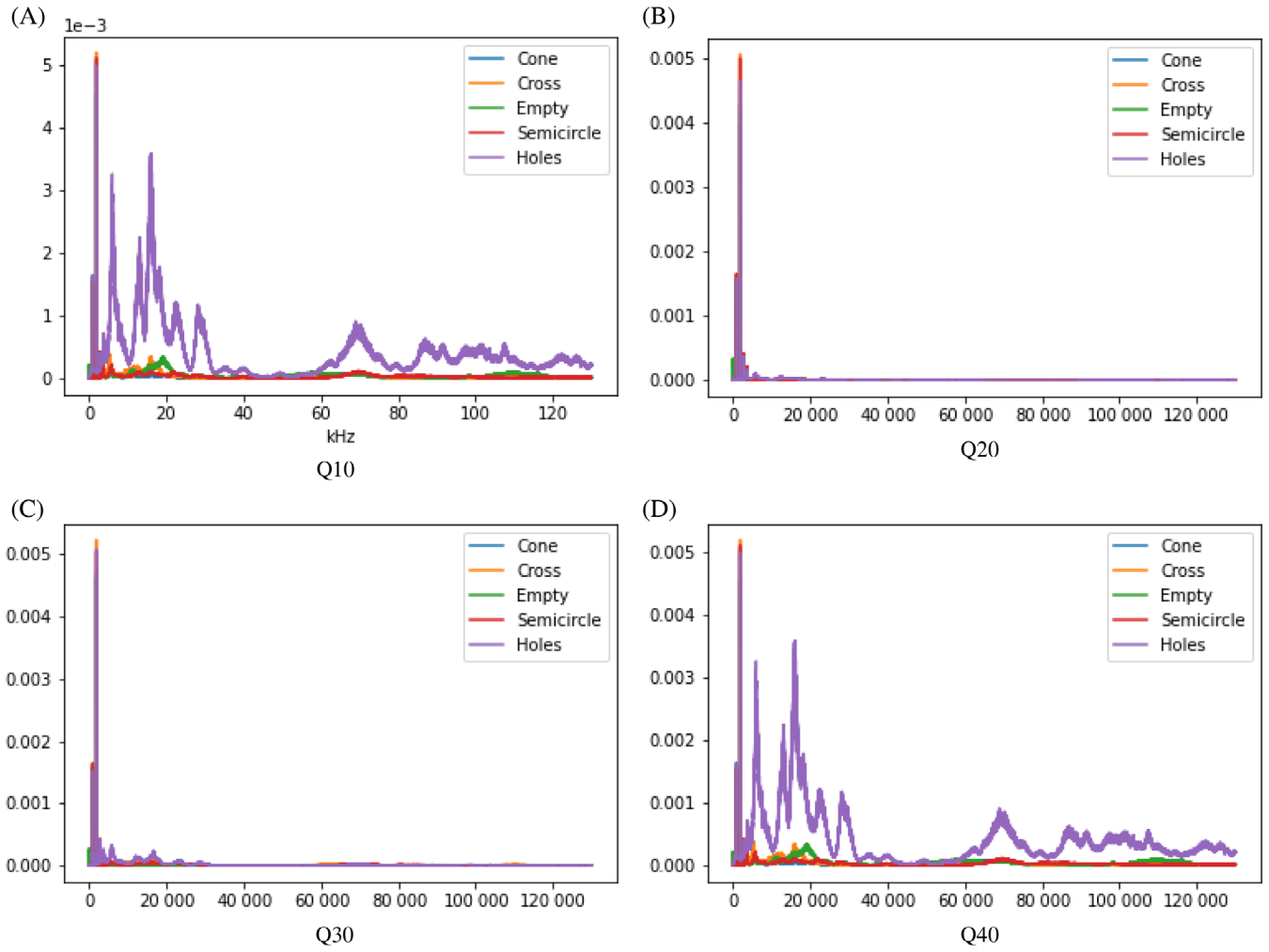

FIGURE B5 Inter-class difference, in the form of column-wise median, of the 200 experiments for each class at different flow rates